Nuclear Instruments and Methods in Physics Research A 806 (2016) 14–20

Contents lists available at ScienceDirect

Nuclear Instruments and Methods in Physics Research A

journal homepage: www.elsevier.com/locate/nima

Neutron beam monitoring for time-of-flight facilities with gaseous detectors

Eleni Aza [a,b,*], Matteo Magistris [a], Fabrizio Murtas [a,c], Silvia Puddu [a,d], Marco Silari [a]

[a] CERN, Geneva 23, 1211 Geneva, Switzerland
[b] AUTH, Department of Physics, 54124 Thessaloniki, Greece
[c] LNF-INFN, Via Fermi 40, 00044 Frascati, Italy
[d] AEC-LHEP, University of Bern, Sidlerstrasse 5, 3012 Bern, Switzerland

ARTICLE INFO

Article history:
Received 4 September 2015
Accepted 16 September 2015
Available online 9 October 2015

Keywords:
Neutron beam monitor
Gaseous Detector
Time-of-flight method
Beam profile

ABSTRACT

Triple Gas Electron Multipliers (GEM) for slow and fast neutrons were employed at the n_TOF facility at CERN as online beam imaging monitors and for energy spectra measurements via the time-of-flight technique. The detectors were exposed to the neutron spectrum ranging from thermal to 1 GeV, produced by spallation of 20 GeV/c protons in a lead target with a maximum intensity of $7 \cdot 10^{12}$ protons per pulse. The spectrum and the 2D count distribution of the neutron beam were measured and compared at two distances from the target, 185 m and 200 m. The detectors showed radiation hardness, linear response and the ability to monitor the beam profile online with high spatial resolution.

1. Introduction

Neutron time-of-flight facilities such as n_TOF [1] at CERN and LANSCE [2] at LANL are commonly employed for studying neutron induced reactions for nuclear structure and reaction physics [3], astrophysics [4], nuclear technology [5] and detector characterization [6]. These facilities typically feature white neutron sources produced by spallation through protons impinging on heavy targets. The neutron energy is determined by measuring the time-of-flight over a known path. The neutron beam characteristics need to be continuously monitored in terms of spot dimensions and energy spectrum at the experimental areas.

In this study the triple Gas Electron Multiplier (GEM) [7] is investigated as a neutron beam monitor, able to measure the energy spectrum via the time-of-flight technique and monitor online the 2D count distribution of the neutron beam spot. Detectors for slow and fast neutrons were tested at the n_TOF facility at CERN; this facility features a neutron source produced by spallation on a lead target by 20 GeV/c protons from the Proton Synchrotron (PS) with a maximum intensity of $7 \cdot 10^{12}$ protons per pulse, with typically a few pulses per minute. The neutrons so produced travel inside a large beam pipe and arrive at two experimental areas, called EAR1 and EAR2, located at 185 m and 20 m from the target, respectively. Measurements can also be performed right before the EAR1 beam dump, located 200 m from the target. Due to the long flight path and short proton pulse, the time-of-flight defines the neutron kinetic energy; the spectrum produced ranges from 10^{-3} eV to 1 GeV (see Fig. 1). The spectrum shows an intense evaporation peak at 1 MeV, a high energy peak at 100 MeV and a thermal peak with lower intensity.

2. Experimental set-up

The triple GEM consists of three insulating kapton foils, clad on both sides with thin metal layers and sandwiched between two electrodes, a cathode and an anode, creating four regions inside the detector: a drift region, two transfer regions and an induction region. The foils are perforated with a large number of holes, acting as multiplication channels for electrons released by ionizing radiation in the gas mixture. If a suitable voltage is applied to the foils, a strong electric field is generated inside the holes, so that electrons can acquire enough energy to develop an avalanche. The signal generated by the electron cascade is induced on a padded anode.

Three triple GEM detectors were tested for slow and fast neutrons. The first one for slow neutrons, named GEM ^{10}B and described in detail in [8,9], has an active area of 5×5 cm^2 and glass sheets coated with a thickness of 300 nm of ^{10}B on both sides. The second detector for slow and fast neutrons has an active area of 10×10 cm^2 and a 1 μm B_4C cathode [10]. The fast neutron detector [11], equipped with 60 mm polyethylene (PE) and 40 mm aluminium, has an active area of 10×10 cm^2. The voltage is applied by a HVGEM NIM module [12]; the values of fields, high

* Corresponding author at: CERN, Geneva 23, 1211 Geneva, Switzerland.
E-mail address: eleni.aza@cern.ch (E. Aza).

http://dx.doi.org/10.1016/j.nima.2015.09.054
0168-9002/

voltages and currents are instantaneously monitored by nanoammeters integrated in the HVGEM. A set of eight CARIOCA-GEM CHIPs [13] shape and digitize the signals induced on 128 pads. An FPGA motherboard collects the signals and counts them in several time windows without any dead time. More information about the acquisition system can be found in [14]. The detectors were filled with a gas mixture of Ar/CO_2 (70/30) and their characteristics and measurement positions are summarized in Table 1.

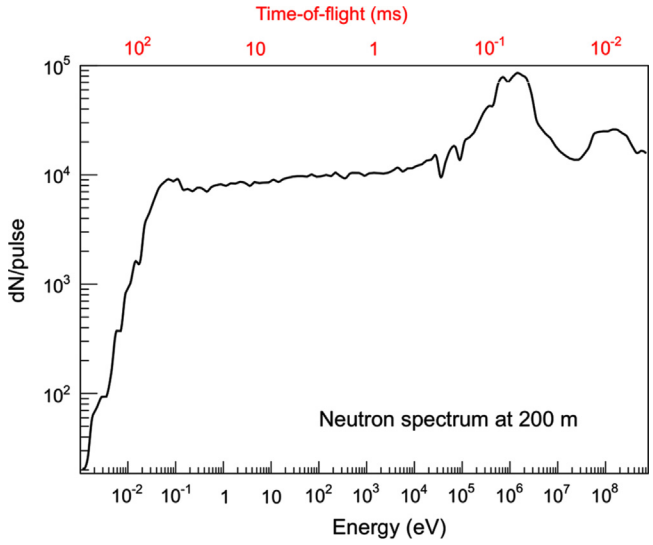

Fig. 1. n_TOF neutron spectrum at the EAR1 beam dump 200 m from the target, taken from [1].

Table 1
Summary of detector characteristics and measurement positions.

Detector	Area (cm^2)	Pad size (mm^2)	Position (m)	Energy
GEM ^{10}B	5×5	3×6	185	Slow
GEM B_4C	10×10	8×8	200	Slow, Fast
GEM PE	10×10	8×8	200	Fast

The detectors GEM B_4C and GEM PE were placed at a distance of 200 m from the target, between the end of the beam pipe and the dump (Fig. 2a). They were mounted on a stand and remotely centred by means of a rail, so that the beam impinged vertically to the foils. The FPGA-based motherboard used to analyse the signal coming from the read-out chips was placed off-beam in order to avoid possible interruptions due to the high beam flux, observed in previous measurements [14]. The GEM ^{10}B was tested inside EAR1 at a distance of 185 m (Fig. 2b). Since it is a side-on detector, the beam impinges parallel to the foils through the window.

3. Time of flight measurements

Time-of-flight measurements were performed via the FPGA-based motherboard, externally triggered a few μs before the proton beam hit the target. The beam energy spectrum was measured from the neutron time-of flight, using the classical kinetic energy formula for energy below 1 MeV and the relativistic one above 1 MeV. The time-of-flight ranged from 700 ns for 1 GeV to 150 ms for thermal neutrons, calculated from the following equations:

$$E_n = \frac{1}{2}mv^2,\ E_n < 1\ \text{Mev}$$

$$E_n = mc^2(\gamma - 1),\ \ \gamma = \left(1 - \frac{v^2}{c^2}\right)^{-\frac{1}{2}},\ E_n > 1\ Mev$$

where c is the velocity of light and v is the neutron velocity ($v = L/t$ with L being the distance from the target and t the time-of-flight).

Two different acquisition methods were employed by means of the FPGA: the multi-slice and the delay scan methods for slow and fast neutrons, respectively. The multi-slice method allowed measuring up to 250 successive time gates of the same width at once, without dead time between them and with a minimum width of 30 μs each. The delay scan method was performed by increasing the acquisition delay with a step equal to the time gate. The minimum gate width is 20 ns.

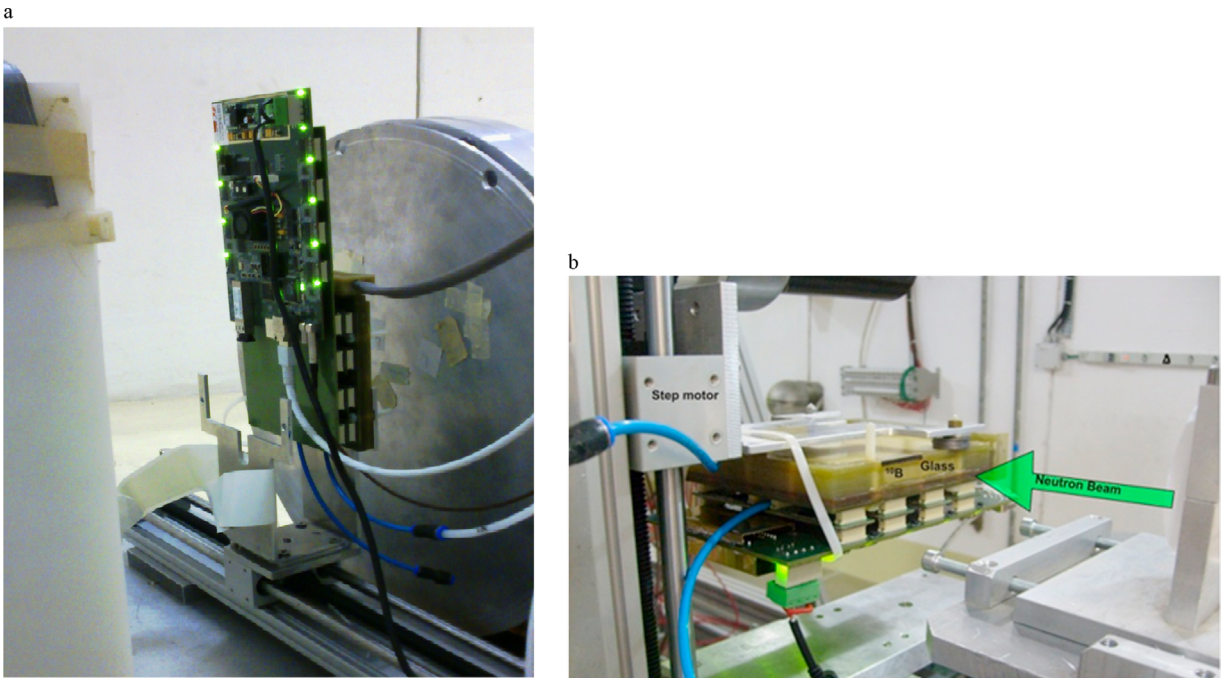

Fig. 2. Experimental set-up at 200 and 185 m respectively. (a) The head-on detectors GEM B_4C and PE were placed at a distance of 200 m, between the end of the beam pipe and the dump. (b) The side-on detector GEM ^{10}B was tested at 185 m, inside the Experimental Area 1 (EAR1).

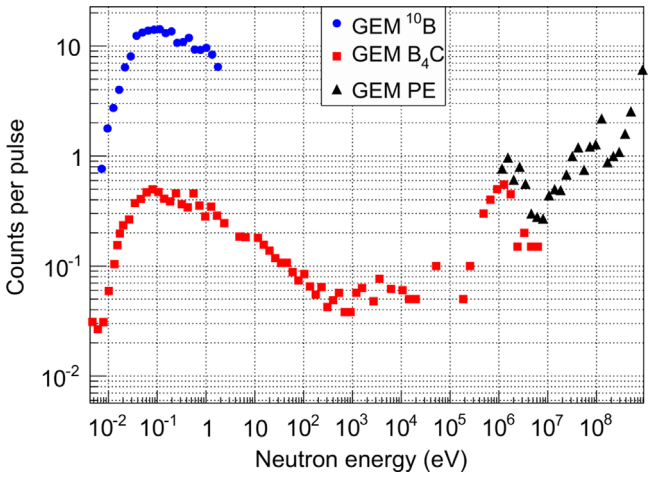

Fig. 3. Number of counts per pulse measured with the detectors GEM ^{10}B, B_4C and PE for increasing energy.

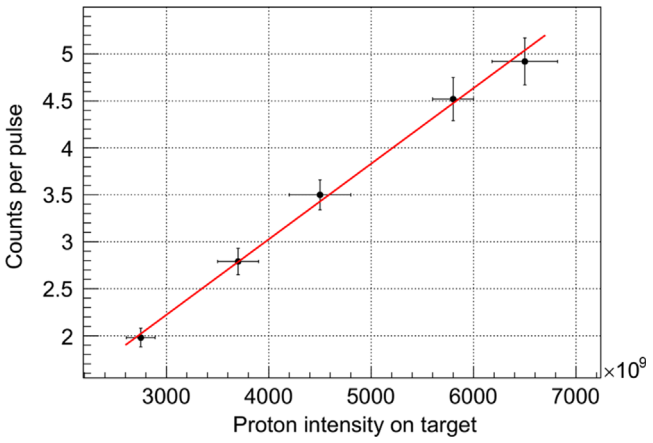

Fig. 4. Correlation plot between measured counts and proton intensity for GEM B_4C.

The data for GEM ^{10}B were acquired in 150 slices for a gate of 1 ms width for each slice. A delay of 10 ms was applied, so that the measured energy ranged from thermal energy (25 meV) to 2 eV (Fig. 3). Measurements with GEM B_4C were performed in two stages: 200 slices of 0.05 ms each were acquired in the range 2 eV to 10 MeV and 400 slices from thermal energy to 2 eV with a gate of 0.5 ms. A delay scan of 100 ns gate was performed for fast neutron measurements with GEM PE, resulting in 154 steps for the energy range 1 MeV to 1 GeV. The number of counts measured per spill for increasing neutron energy is shown in Fig. 3 for GEM ^{10}B, B_4C and PE. The average number of protons impinging on the target for these acquisitions was $(6.5 \pm 0.3) \cdot 10^{12}$ per pulse. The efficiency difference between GEM ^{10}B and GEM B_4C stems from the different cathode geometry and material: the first employs 10 layers of ^{10}B while the second only one layer of B_4C.

Good correlation was found between the total number of counts measured with GEM B_4C and proton intensity on target varying from $2 \cdot 10^{12}$ to $7 \cdot 10^{12}$ per spill. The detector showed a linear response (Fig. 4), with a ratio of $(8.0 \pm 0.4) \cdot 10^{-13}$ counts per proton on target per pulse. The total number of counts acquired for the highest proton intensity was 4.9 ± 0.3 per pulse for thermal up to 10 keV neutrons.

3.1. Efficiency to neutrons

The efficiency for thermal neutrons of GEM ^{10}B was measured previously [8] as $4.3 \cdot 10^{-2}$. The present time-of-flight measurements gave the opportunity to measure it in shorter energy ranges (Fig. 5a), yielding a value of $(4.2 \pm 0.2) \cdot 10^{-2}$ for thermal neutrons, by dividing the counts measured per bin by the estimated number of neutrons [1]. The efficiency decreases for increasing neutron energy following the trend of the reaction cross-section ^{10}B$(n,\alpha)^7$Li.

The GEM PE efficiency was measured in the past [11] at the Frascati Neutron Generator (FNG, ENEA-Frascati) [15] as $3.8 \cdot 10^{-5}$ for 2.5 MeV neutrons. In the present study it was measured as $(4.8 \pm 0.3) \cdot 10^{-5}$ for the same energy; the efficiency function was further extended up to 200 MeV (Fig. 5b). The average efficiency in the range of 2–20 MeV was measured as $(1.3 \pm 0.1) \cdot 10^{-4}$, while it was simulated in the past as $1.2 \cdot 10^{-4}$ [11] using the GEANT4 Monte Carlo code [16] and in the present study as $(1.3 \pm 0.1) \cdot 10^{-4}$ with the FLUKA Monte Carlo code [17,18]. The simulation consisted of a monoenergetic rectangular neutron beam impinging on the active area of the GEM PE detector. The efficiency was estimated as the number of charged particles entering the drift region and depositing energy that corresponds to charge exceeding the electronics threshold, normalized per impinging neutron. The efficiency as a function of the neutron energy is shown in Fig. 5b for the measurement and the FLUKA simulation, showing a maximum value of $(3.3 \pm 0.2) \cdot 10^{-4}$ in the energy bin 5–6 MeV.

The GEM detectors have a good efficiency for neutron detection, with high rejection factor for photons (i.e. about 10^{-7} for a voltage corresponding to a chamber gain of 300 [19]). By setting suitable values of threshold and voltage, the electronic noise can be significantly reduced and a good compromise between gamma rejection and neutron efficiency can be obtained. In particular, the electrons generated by photons ionize much less than the charged particles (protons, alpha particles and lithium ions) produced by neutrons, and will typically produce an analogue signal that does not exceed the threshold.

3.2. Prompt and delayed photon flash

A detailed simulation of the particle spectrum arriving at the n_TOF beam dump was performed in the past [20] with FLUKA. Apart from neutrons and charged particles, a high flux of prompt and delayed photons with a spectrum ranging from several keV to several GeV arrives at 200 m. This flux of 10^{11} cm^{-2} s^{-1} is high enough for the photon signal to be detected despite the high rejection factor. The photon flash was measured with the GEM B_4C applying 900 V (gain 300) and performing a delay scan of 50 ns width. The time-window of prompt photons is 300 ns (2100–2400) ns arrival time as shown Fig. 6), after which delayed photons are detected. This window overlaps with the neutron time-of-arrival up to 300 MeV and therefore the neutron spectrum cannot be measured above this energy without the photon contamination.

The number of counts per pulse of the prompt flash was measured for increasing proton intensity and different voltages. For an applied voltage of 900 V the response was found linear (see Fig. 7). By applying a higher voltage of 1050 V, the photon signal is amplified and deviation from linearity appears at 600 counts (see Fig. 7), corresponding to $2 \cdot 10^7$ counts cm^{-2} s^{-1} or $1.3 \cdot 10^7$ counts s^{-1} per channel in the 300 ns time-window, due to saturation effects on the read-out electronics. The photon rejection factor was estimated as 10^{-5} for 900 V and 10^{-4} for 1050 V in the intensity range where the detector shows linear response. The difference from previous measurements [19] stems from the different photon energy measured: in [19] the detector was tested with ^{22}Na and ^{60}Co sources while at n_TOF the photon flash shows a wide energy spectrum.

The saturation effect was observed also in the 2D image of the beam. During the measurement a screenshot of the Labview console was taken for these two voltages (see Fig. 8): the photon flash at 900 V (Fig. 8a) follows a Gaussian distribution, while at 1050 V

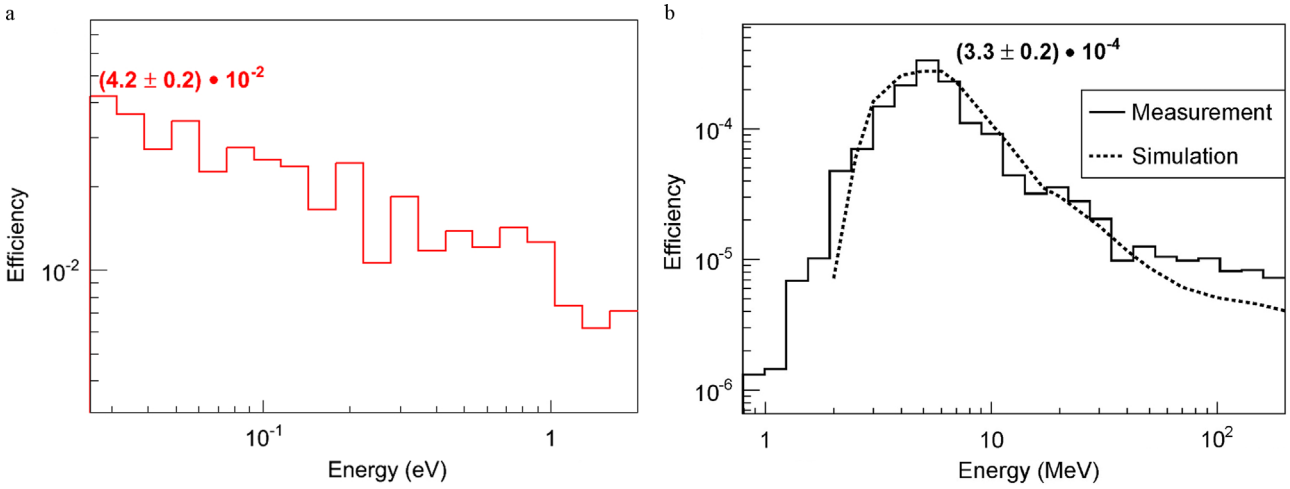

Fig. 5. Efficiency of GEM ^{10}B and GEM PE measured in the corresponding energy ranges. (a) The efficiency of GEM ^{10}B decreases for increasing neutron energy. (b) The efficiency of GEM PE increases, reaching a maximum at 5–6 MeV. A simulation with FLUKA is shown for comparison.

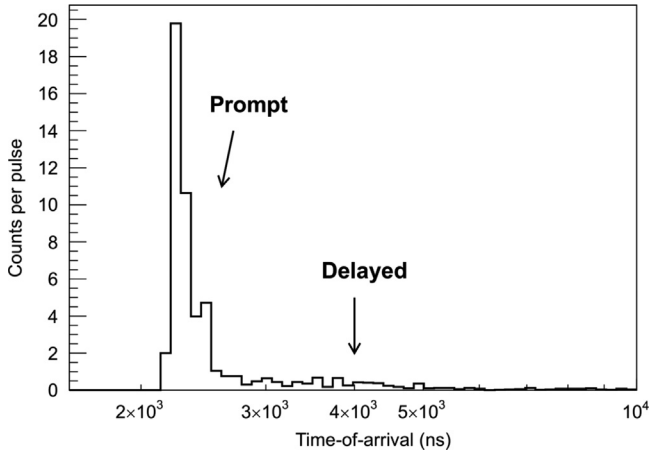

Fig. 6. Time-of-arrival of the prompt and delayed photon flash measured with the GEM B_4C at 900 V.

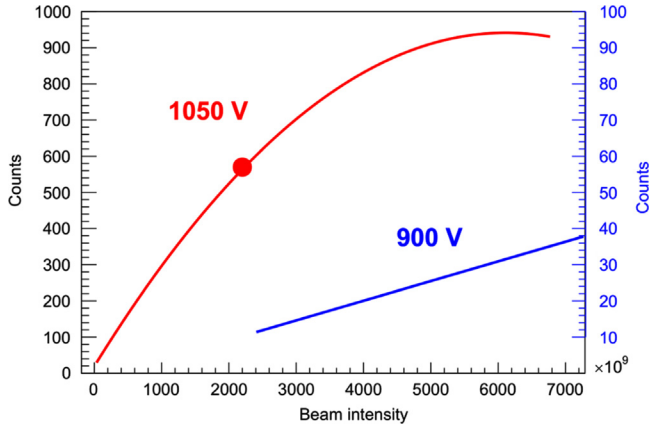

Fig. 7. Number of counts for increasing beam intensity measured with the GEM B_4C for 1050 V and 900 V voltage applied. The detector saturates for 1050 V, while its response is linear for 900 V.

(Fig. 8b) it shows an annular distribution. The low number of counts in the centre of this distribution indicates the saturated channels. The colour scale on the right of the figures indicates the total number of counts per pad for a given number of events, which is not the same for the two acquisitions.

4. Beam profile at n_TOF

The beam profile was measured with the three GEM detectors, see Table 1, at EAR1 (185 m) and at the beam dump (200 m). Even though the neutron energy spectrum in Fig. 1 arriving at these positions should not differ significantly, the beam dimensions are expected to increase for the additional 15 m flight path due to diffusion of slow neutrons.

4.1. Profile at EAR1

The GEM ^{10}B was employed for neutron beam imaging at EAR1. Since it is a side-on detector and the beam is larger than the detector window, a horizontal and a vertical scan were performed with a step motor in order to measure the entire image. The GEM was fixed on a step motor (Fig. 2b) and the two scans were performed with 15 steps, each one displaced by 3 mm from the previous one.

The following procedure was used in order to reconstruct the image of the thermal neutron beam:

1. Two matrices, V_{ij} for the vertical and H_{ij} for the horizontal scan, were created and the peak of each count distribution was centred at position (20, 20) cm of each matrix (see Fig. 9).
2. The two matrices were summed to obtain the matrix $S_{ij}=V_{ij}+H_{ij}$.
3. The matrix S_{ij} was weighted by the entries of another matrix D, composed of values 0.5 and 1. Value 0.5 was placed in the bins where there was overlapping of the matrices V_{ij} and H_{ij}, while number 1 was placed in the rest of the bins. Applying this method, it was possible to obtain the arithmetic mean from counts of overlapping bins and the sum from non-overlapping bins.

The reconstructed beam image, which follows a Gaussian distribution with $\sigma_x=6.5$ mm and $\sigma_y=6.0$ mm, is shown in Fig. 10.

4.2. Profile at the beam dump

The beam image at the dump (200 m) was measured with the GEM B_4C and the GEM PE. Both detectors are head-on with a 10×10 cm^2 active area; therefore it was possible not only to acquire the image at once but also to visualize it online via the Labview based console. A screenshot of the console is shown in Fig. 11, with its four panels: (A) and (B) show the instantaneous

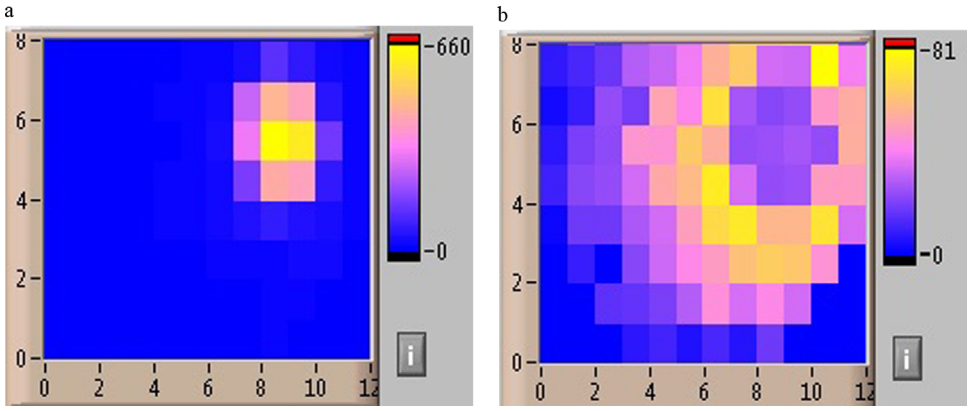

Fig. 8. Screenshot of the online acquisition system measuring the photon flash for (a) 900 V and (b) 1050 V voltage applied.

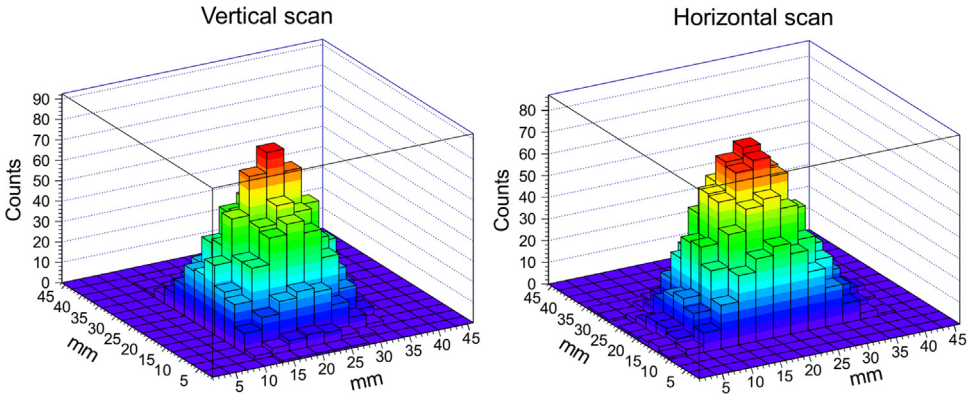

Fig. 9. Vertical and horizontal scans with 3 mm steps. The count distribution peaks were moved to position (20, 20) cm in the matrices.

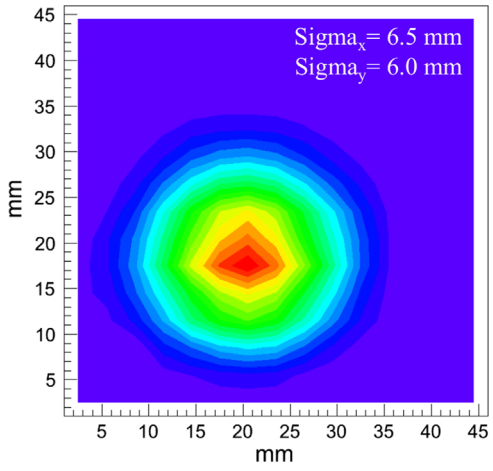

Fig. 10. Beam profile measured with the GEM ^{10}B at 185 m. The distribution is fitted with a Gaussian function and the sigma in *x* and y directions is 6.5 mm and 6.0 mm, respectively.

and accumulated count distributions on the pads and (C) and (D) the respective vertical and horizontal distribution profiles.

The images measured with both detectors are shown in Fig. 12a and b. The beam spot for slow neutrons (Fig. 12a) is larger than the one for fast neutrons (Fig. 12b), due to the higher diffusion of the former when they travel inside the beam pipe. In addition, the slow neutron spot is shifted by approximately 1.5 cm in the vertical direction due to the effect of gravity. A significant increase in the beam dimensions of the low energy component is also evident for an additional flight path of 15 m. According to simulations performed for the beam dimensions at 185 m and 200 m [21], the spot diameter was simulated as 4.8 ± 0.2 cm and 10.6 ± 0.2 cm, respectively, and it was measured here as 4.0 ± 1.2 cm and 8.7 ± 1.6 cm. The present results are in fair agreement with the simulations, given the large measurement uncertainty stemming from the pad size. The fast component of the beam spot at 200 m was measured in the past [22] with another GEM PE (6×12 mm^2 pad size) and was found to have the same dimensions.

The beam image at the dump was additionally measured in different energy ranges by selecting the corresponding time-of-flight, in order to determine possible differences in dimensions. The sigma of the fitted Gaussian distribution measured with the GEM B_4C in the horizontal (*x*) and vertical (*y*) directions is presented in Table 2 for four energy ranges. It is evident that the size of the beam increases significantly in the thermal region (0.01–0.05 eV), an effect mostly concerning the *x* direction.

5. Conclusions

Three triple GEM detectors with different active area and readout pad size were employed for measuring the energy spectrum and spot dimensions of the neutron beam at CERN n_TOF facility. By means of an externally triggered FPGA-based motherboard it was possible to measure the neutron time-of-flight and spectrum at two distances from the target, 185 and 200 m, using time gates of 100 ns and 50 μs for fast and slow neutrons, respectively.

The GEM B_4C showed linear response to neutrons from thermal energy to 10 keV and for increasing proton intensity on target, measuring $(8.0 \pm 0.4) \cdot 10^{-13}$ counts per proton on target per pulse. The prompt and delayed photon flash was measured with the same detector, as photons reached the measurement position right after the spallation process in the lead target.

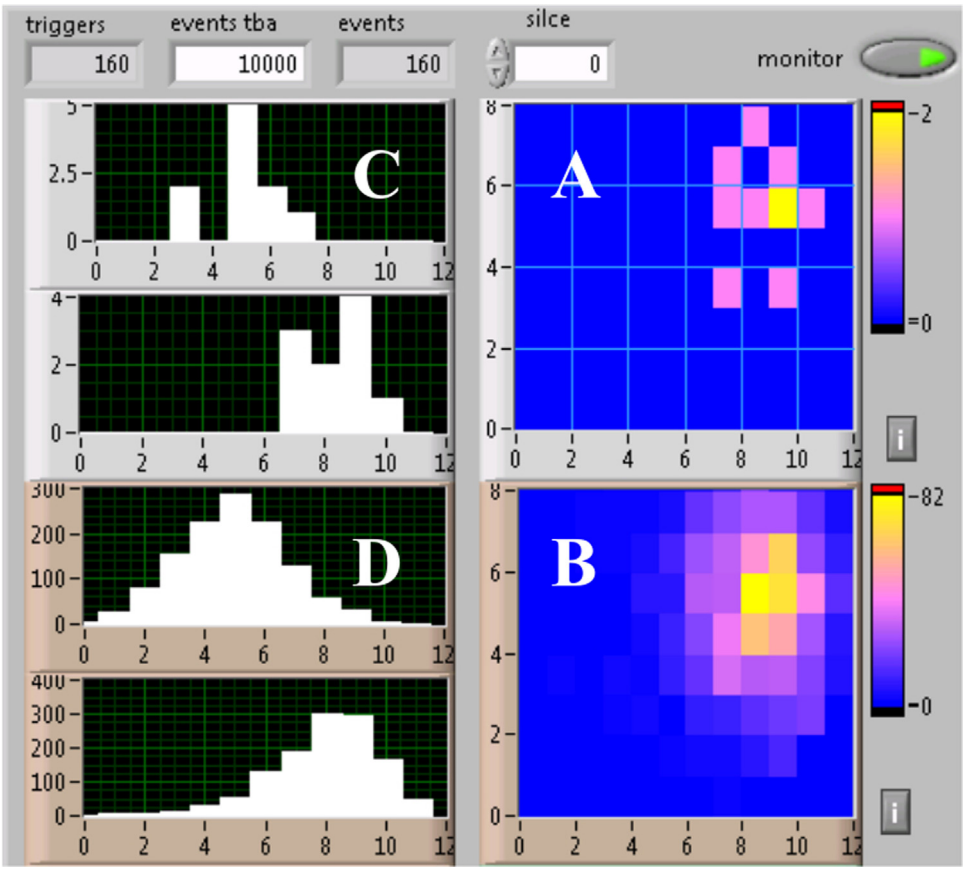

Fig. 11. Screenshot of the Labview console used to operate the detector. The instantaneous (A, C) and accumulated count distributions (B, D) on the pads can be visualized online.

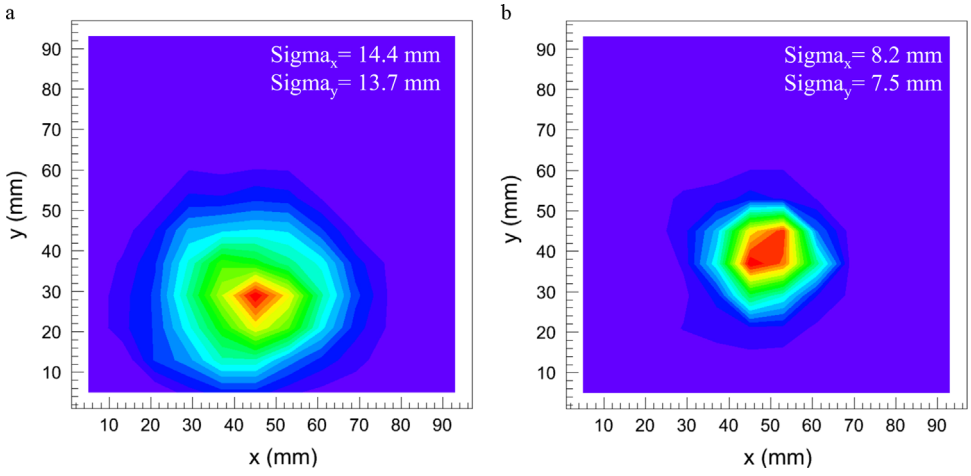

Fig. 12. Beam profile measured with the (a) GEM B_4C and (b) GEM PE at 200 m. The beam spot is larger for the slow neutron component and shifted in the vertical direction.

Table 2
Sigma in the x and y directions of the fitted beam distribution for different energy ranges, measured with the GEM B_4C.

Range (eV)	Sigma x (mm)	Sigma y (mm)
0.01–0.05	16.1 ± 0.3	13.9 ± 0.2
0.05–2	14.8 ± 0.2	13.8 ± 0.2
2–8	14.4 ± 0.2	13.7 ± 0.2
8–10	14.3 ± 0.1	13.6 ± 0.2

The 2D beam spot inside the EAR1 (185 m) was measured with the GEM ^{10}B in the neutron energy range from thermal to 2 eV, by means of horizontal and vertical scans of 3 mm steps. The sigma of the Gaussian distribution in the x and y directions was found as $\sigma_x = 6.5$ mm and $\sigma_y = 6.0$ mm. In front of the beam dump (200 m) the spot was measured with the GEM B_4C in the range from thermal to 10 keV, showing larger dimensions with $\sigma_x = 14.4$ mm and $\sigma_y = 13.7$ mm. The fast component of the beam, from MeV to 1 GeV,

was measured at the same position with the GEM PE and the spot characteristics were $\sigma_x = 8.2$ mm and $\sigma_y = 7.5$ mm. Due to the acquisition system employed, the 2D count distribution and the profiles in both directions at 200 m could be monitored online with a spatial resolution corresponding to the read-out pad size (8 mm).

The present study shows that the triple GEM detector can be employed as an online beam monitor in a neutron time-of-flight facility, measuring the energy spectrum in a single acquisition and the 2D count distribution in specific energy ranges.

Acknowledgments

The authors would like to thank the n_TOF Collaboration for the significant help provided during the measurements.

This research project has been supported by the Marie Curie Initial Training Network Fellowship of the European Community's Seventh Framework Program under Grant Agreement PITN-GA-4 2011-289198-ARDENT.

References

[1] C. Guerrero, et al., European Physical Journal A 49 (2013) 27.
[2] P.W. Lisowski, K.F. Schoenberg, Nuclear Instruments and Methods A 562 (2006) 910-91914.
[3] F. Gunsing et al. Neutron resonance spectroscopy at n_TOF at CERN, In: International Conference on Nuclear Data for Science and Technology, 2007. http://dx.doi.org/10.1051/ndata:07690.
[4] F. Kappeler, Progress in Particle and Nuclear Physics 43 (1999) 419.
[5] W. Gudowski, Nuclear Physics A 654 (1999) C436.
[6] B. Bergmann, et al., Journal of Instrumentation 9 (48, 2014) C050.
[7] F. Sauli, Journal of Instrumentation A386 (1997) 531.
[8] A. Pietropaolo, et al., Nuclear Instruments and Methods 729 (2013) 117–126.
[9] E. Aza, et al., Journal of Instrumentation 9 (2014) T11005.
[10] F. Murtas, Journal of Instrumentation 9 (2014) C01058.
[11] F. Murtas, Journal of Instrumentation 7 (2014) P07021.
[12] F. Murtas, et al., Nuclear Instruments and Methods in Physics Research A572 (2007) 96–97.
[13] W. Bonivento, et al., Nuclear Instruments and Methods in Physics Research A 491 (2002) 233–243.
[14] E. Aza, et al., Journal of Instrumentation 9 (2014) P06006.
[15] M. Martone, et al., Journal of Nuclear Materials B (1994).
[16] S. Agostinelli, et al., Nuclear Instrum. Methods A506 (2003).
[17] A. Ferrari, P.R. Sala A. Fasso J. Ranft FLUKA: a multi-particle transport code, CERN 2005–10, INFN/ TC_05/11 SLAC-R-773.
[18] T.T. Bohlen, F. Cerutti, M.P.W. Chin, A. Fasso, A. Ferrari, P.G. Ortega, A. Mairani, P.R. Sala, G. Smirnov, V. Vlachoudis, Nuclear Data Sheets 120 (2014) 211–214.
[19] G. Croci, et al., Journal of Instrumentation 8 (2013) P04006.
[20] C. Borcea et al., 2000. Particle distributions, entering the vacuum tube, from an 80x80x60 cm^3 lead target CERN SL-Note-2000-029 EET.
[21] A.Tsinganis, Private communication.
[22] G. Claps, et al., 2012. Performance test of triple GEM detectors at CERN n_TOF facility, IEEE, Conference Record.